A Strengthened Influence of ENSO on August High Temperature Extremes over the Southern Yangtze River Valley since the Late 1980s

KAIMING HU

Center for Monsoon System Research, Institute of Atmospheric Physics, Chinese Academy of Sciences, Beijing, China

GANG HUANG

Key Laboratory of Regional Climate–Environment for East Asia, Institute of Atmospheric Physics, Chinese Academy of Sciences, Beijing, China

RENGUANG WU

Institute of Space and Earth Information Science, and Department of Physics, Chinese University of Hong Kong, Hong Kong, China

(Manuscript received 15 May 2012, in final form 7 September 2012)

ABSTRACT

The present study investigates the decadal change in the relationship between China high temperature extremes (HTEs) and El Niño–Southern Oscillation (ENSO). It is found that the relationship between the August HTEs in the southern Yangtze River valley (SYRV) and ENSO has strengthened since the late 1980s. Before the late 1980s, the relationship is weak, whereas, after the late 1980s, the August hot-day numbers in the SYRV region tend to be more than normal during El Niño decaying years. During 1988–2008, El Niño–induced August warm SST anomalies are mainly located in the eastern tropical and north Indian Ocean. As a response to the north Indian Ocean warming, the South Asia high extends eastward, and the SYRV is overlain by upper-level easterly anomalies. The cold horizontal temperature advection induced by upper-level easterly anomalies leads to anomalous descent, which is conducive to the occurrence of HTEs through adiabatic warming. During 1966–86, El Niño–induced August warm SST anomalies are mainly distributed in the equatorial central and southwest tropical Indian Ocean. Corresponding to the equatorial Indian Ocean warming, the ascending motion over the Arabian Sea is enhanced, which leads to an anomalous anticyclone over the Middle East through a Rossby wave–type response and in turn an anomalous cyclone over China through a midlatitude wave pattern. The SYRV is controlled by upper-level westerly anomalies, which is not conducive to the occurrence of HTEs since the corresponding horizontal temperature advection and anomalous vertical motion are weak. As such, the impact of ENSO on August SYRV HTEs is weak before the late 1980s.

1. Introduction

In recent years, high temperature extremes (HTEs) have received increasing concerns because of their adverse effects on human and natural systems (Easterling et al. 2000). The HTEs can affect human health and life, energy supply and demand, water resources, and agricultural production. A well-documented example is the European heat wave of 2003, which resulted in 22 000–35 000 heat-related deaths and major financial losses (Schär and Jendritzky 2004). In the densely populated eastern part of China, the effects of HTEs are very serious. For instance, daily mortality was significantly above normal in Shanghai when hot waves occurred in the summer of 1998 and 2003 (Tan et al. 2007).

In China, the HTEs not only have experienced remarkable long-term changes (Zhai et al. 1999; Wei and Chen 2011) but also have significant interannual variability (Wei and Chen 2009) in recent decades. By analyzing the number of hot days ($T_{max} > 35°C$) in China during the period 1959–2008, Wei and Chen (2009) revealed that the average and standard deviation of the

Corresponding author address: Gang Huang, RCE-TEA (Key Laboratory of Regional Climate–Environment for East Asia)/IAP (Institute of Atmospheric Physics)/CAS (Chinese Academy of Sciences), P.O. Box 9804, Beijing 100029, China.
E-mail: hg@mail.iap.ac.cn

DOI: 10.1175/JCLI-D-12-00277.1

number of hot days were the largest over the lower reaches of the Yangtze River, with a maximum of 25 days and a standard deviation of 15 days. The large interannual variability of hot-day numbers indicates that this region is prone to high temperature disaster. Thus, understanding the causes for the occurrence of HTEs has great benefit to the society and economy.

El Niño–Southern Oscillation (ENSO) is one important factor for climate anomalies in China (Fu and Ye 1988; Huang and Wu 1989; Wu et al. 2003). ENSO affects the climate over China through its influence on the northwest Pacific (NWP) subtropical high (Zhang et al. 1996; Wang et al. 2000; Li et al. 2008; Xie et al. 2009), the South Asian high (Yang et al. 2007; Huang et al. 2011), and the midlatitude wave train (Wu and Wang 2002; Ding and Wang 2005). Recently, using the observational data during the period 1979–2008, Hu et al. (2012) demonstrated that ENSO can affect the HTEs in China through an anomalous NWP anticyclone. During El Niño's decaying phase, El Niño–induced tropical Indian Ocean warming induces a low-level anomalous anticyclone over the NWP in summer (Xie et al. 2009), which leads to above normal hot days in the southern Yangtze River valley (SYRV) in late summer through descent-related adiabatic warming and reduced rainfall. However, the relationship between the East Asian climate and ENSO is not stable. For example, decadal changes in the late 1970s have been identified in the relationship between ENSO and East Asia rainfall (Xie et al. 2010; Huang et al. 2010) and temperature (R. Wu et al. 2010; Hu et al. 2011). Because of the harmful impacts of the HTEs, it is necessary to investigate whether the relationship between ENSO and China HTEs has experienced decadal changes. Such decadal change is relevant to the prediction and mitigation of the high temperature disaster.

The primary focus of this study is to document the decadal change in the relationship between ENSO and China HTEs and its possible mechanisms. This paper is organized as follows: The datasets are described in section 2. The observational evidence for the decadal change in the relationship between China HTE and ENSO is shown in section 3. The possible mechanism for the decadal change is analyzed in sections 4–6. A summary of the results is provided in section 7.

2. Data

The China daily maximum surface temperature used in this study is from an updated homogenized daily maximum and minimum temperature dataset for 549 Chinese stations during 1960–2008 (Li and Yan 2009). This dataset was developed using the multiple analysis of series for homogenization software package, which can be used to detect all the major breakpoints caused by nonnatural changes in the long time series and meanwhile make adjustments to homogenize the whole dataset. Following Zhai et al. (1999), we define a hot day when the maximum temperature exceeds 35°C in this study. We also adopted the relative value criteria to define the hot days when the maximum temperature exceeds the 90th or 95th percentile; the results (figure not shown) are the same as those based on the absolute value criterion.

The monthly mean global SST dataset used in this study is the Hadley Centre Sea Ice and Sea Surface Temperature dataset (HadISST1; Rayner et al. 2003). This SST dataset (resolution of $1° \times 1°$) is available from 1870 forward. A Niño-3 SST index was constructed by averaging the December–February (DJF) SSTs over the domain of 5°S–5°N, 90°–150°W. The monthly mean winds, vertical velocity, height fields, and streamfunction fields are derived from the National Centers for Environmental Prediction–National Center for Atmospheric Research (NCEP–NCAR) atmospheric reanalysis with a resolution of $2.5° \times 2.5°$, which is available from 1948 forward (Kalnay et al. 1996).

The present study mainly focuses on the period 1960–2008 in view of the availability of the China daily maximum surface temperature data. A linear trend was subtracted from raw anomalies to remove long-timescale variations.

3. Decadal change in the relationship between August SYRV HTEs and ENSO

Figure 1 shows the correlation of hot-day numbers in summer months with preceding winter [DJF(0)] Niño-3 index during 1960–2008. In June, a weak negative correlation is seen in the eastern part of China and a weak positive correlation is seen in most of northwest China (Fig. 1a). In July, the correlation is still weak (Fig. 1b), but the pattern is obviously different than that in June. There is a positive correlation in the southern and eastern parts of China and a negative correlation in northeast China and the western part of central China. In August, the positive correlation in the SYRV and the coastal region of eastern China reaches the 95% confidence level, with the maximum coefficient exceeding 0.3 (Fig. 1c). Among these 3 months, it is obvious that the relationship between ENSO and China HTEs is most significant in August. Therefore, we mainly focus on the influence of ENSO on August China HTEs in this study.

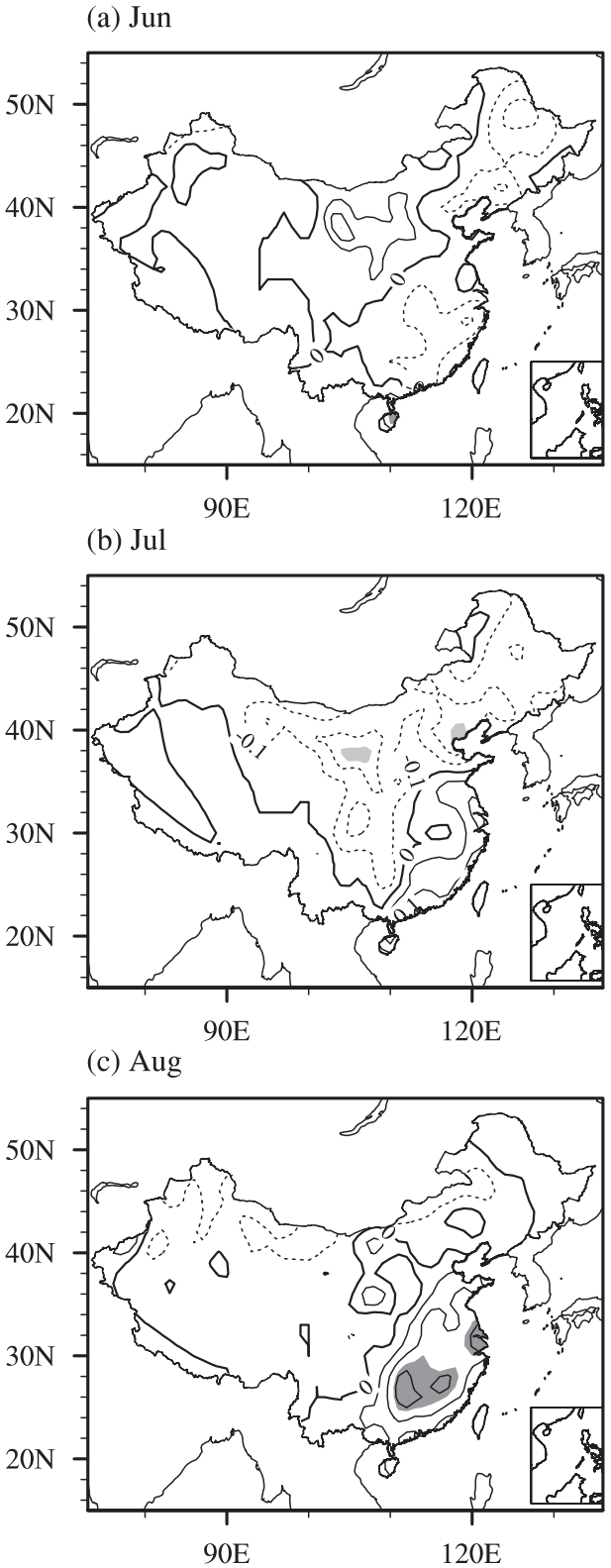

FIG. 1. Correlation of the DJF(0) Niño-3 index with the number of hot days in (a) June, (b) July, and (c) August from 1960 to 2008. The solid lines represent positive correlation, the dashed lines represent negative correlation, and the line interval is 0.1 in correlation. The shaded areas denote correlation reaching the 95% confidence level. The small inset map denotes the region of South China Sea.

To further delineate the relationship between the August HTEs over China and ENSO, we perform a singular value decomposition (SVD) analysis on August hot-day numbers over China and DJF(0) tropical Pacific (30°S–30°N, 90°E–80°W) SST from 1960 to 2008. As shown in Fig. 2, the leading homogeneous SVD mode is characterized by El Niño–like SST anomalies in the tropical Pacific in the preceding winter and more than normal hot-day anomalies over the SYRV in August. This mode accounts for 77% of the total squared covariance. The correlation coefficient between the time series of the corresponding leading SVD modes of DJF (0) SST and August HTEs is 0.42 for the 49-yr period, exceeding the 95% confidence level. The result suggests that the August hot-day numbers in the SYRV region are above (below) normal during El Niño (La Niña) decaying years.

However, the relationship between the August HTEs and ENSO are unstable during the analysis period. This is demonstrated in Fig. 3a, which displays the 15-yr sliding correlation between the time series of the leading SVD mode for China August HTEs (HTE_PC1) and for DJF(0) SST (SST_PC1). For a 15-yr period, correlation coefficients of 0.44 and 0.64 are significant at the 90% and 99% confidence levels, respectively, according to Student's t test. During the 1960s through the 1980s, the correlation is weak. During the 1990s, the correlation is significant, exceeding the 99% confidence level. A notable increase in the sliding correlation is observed during the late 1980s. Using the Mann–Kendall method (Mann 1945), we identified 1987 as the point of abrupt change in the sliding correlation. Thus, we choose 1966–86 and 1988–2008 as the two subperiods in the following analyses. The correlation coefficient between HTE_PC1 and SST_PC1 is 0.26 and 0.68 for 1966–86 and 1988–2008, respectively. Since the HTE_PC1 and SST_PC1 represent the variation of August HTEs in China and ENSO, the above change in the correlation suggests that the relationship between the ENSO and August HTEs in the SYRV region have strengthened since the late 1980s. Indeed, the 15-yr sliding correlation between the area mean number of hot days over the SYRV in August and DJF(0) Niño-3 index shows an obvious increase in the late 1980s (dashed line in Fig. 3a).

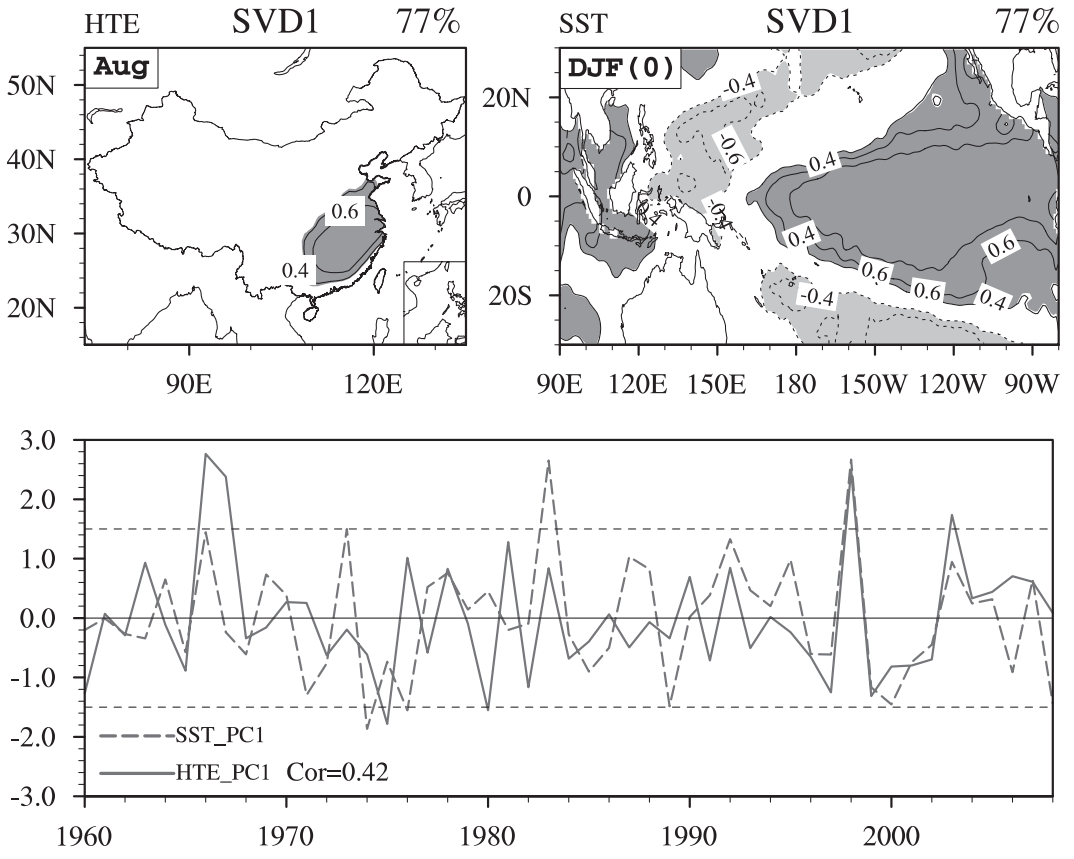

FIG. 2. The first leading SVD homogeneous modes (contours; shading denotes the 95% confidence level) of (top right) the preceding winter SST over Pacific and (top left) the number of hot days in August over China and (bottom) the normalized time series of the first leading SVD mode. The SVD analysis is based on the data from 1960 to 2008. The small inset map denotes the region of South China Sea.

The decadal change in the relationship between ENSO and August HTEs in China is further confirmed by the correlation of the August hot-day numbers over China with the DJF(0) Niño-3 index during the two subperiods (Fig. 4). Apparently, the distribution of correlation coefficient is remarkably different between the two subperiods. During 1966–86, the correlation is weak in the SYRV region. During 1988–2008, significant positive correlation appears in the SYRV region with the maximum correlation coefficient around 0.6.

4. The possible reasons for the decadal change in the relationship between August SYRV HTEs and ENSO

This section investigates the possible reasons for the decadal change in the relationship between August SYRV HTEs and ENSO. First, we document the ENSO-related atmosphere circulation and its change. Then, we discuss the possible reasons for the decadal change in the ENSO-related circulation anomalies. Finally, we investigate the low-level atmospheric warming that resulted from circulation anomalies and its impact on August SYRV HTEs.

a. Change in the ENSO-related circulation anomalies over SYRV in August

To understand the connection from ENSO to the NWP and East Asia circulation and its change, we show in Fig. 5 the regressions of 200-hPa winds (top panels), 500-hPa vertical velocity (middle panels), and 850-hPa winds (bottom panels) in August with a normalized DJF (0) Niño-3 index. During 1966–86, at 850 hPa, there is an anomalous anticyclone over NWP, an anomalous cyclone over midlatitudes extending from Japan to the North Pacific, and an anomalous anticyclone over high latitudes, featuring a meridional wave pattern over NWP. Over the tropical western Pacific, there are easterly anomalies. At 200 hPa, the wind anomalies display a zonal wave structure over the midlatitudes with an

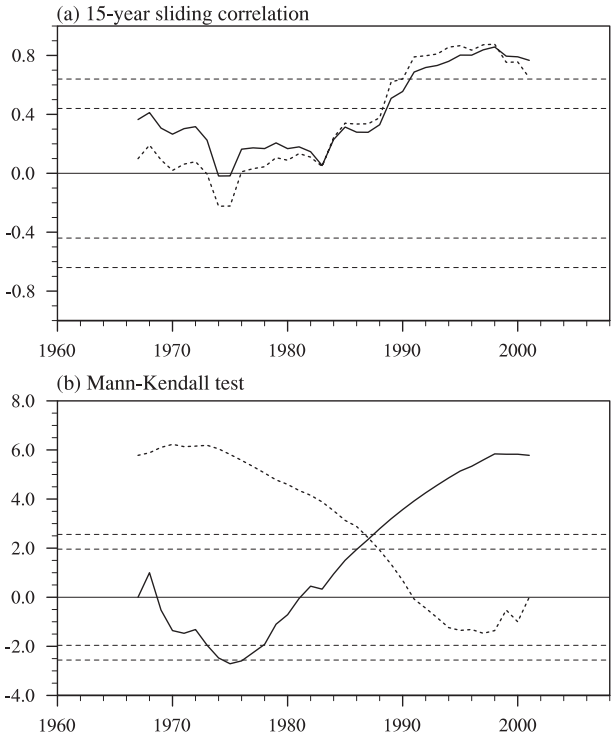

FIG. 3. (a) The 15-yr sliding correlation between the HTE_PC1 (time series of first leading SVD mode for HTEs) and SST_PC1 (time series of first leading SVD mode for SST; solid line) and between the DJF(0) Niño-3 index and the area mean number of hot days over SYRV (25°–31°N, 112°–122°E) in August (dashed line); the dotted horizontal lines denote the 95% and 99% confidence levels, respectively. (b) The Mann–Kendall test for 15-yr sliding correlation between HTE_PC1 and SST_PC1; the dotted horizontal lines represent the 95% and 99.9% confidence levels of the Mann–Kendall test.

anomalous cyclone over China. Over the tropical western Pacific, there are westerly anomalies. The 500-hPa vertical motions display a meridional wave pattern over NWP, consistent with the 850-hPa wind anomalies. Anomalous ascending motion dominates over the tropical Indian Ocean, with maximum anomalous ascent over the western and equatorial Indian Ocean.

During 1988–2008, at 850 hPa, the wind anomalies over the NWP and East Asia feature an anomalous anticyclone over the subtropical NWP through eastern China and an anomalous cyclone over midlatitudes extending from northeast China to Japan. At 200 hPa, the wind anomalies have a large zonal extension in midlatitudes, with significant westerly anomalies along 40°N and easterly anomalies along 20°N and 50°–60°N, an anomalous anticyclone over the subtropics. These features indicate that the South Asia high and the East Asia subtropical jet are strengthened, which is consistent with previous studies (Huang et al. 2011; Qu and Huang 2012a). Over the tropical western Pacific, there exist westerly anomalies. The 500-hPa vertical motions feature a dipole structure over East Asia and the NWP, with significant descending motions extending from the northern part of the Indochinese peninsula to the East China Sea and ascending motions over the middle latitudes of East Asia. Over the tropical Indian Ocean, anomalous ascending motion is present over the eastern and central tropical Indian Ocean.

The ENSO-related circulation anomalies show several important differences between the two subperiods. First, the upper-level wind anomalies are zonally elongated in 1988–2008 but feature a zonal wave structure in 1966–86. Second, the low-level anticyclonic wind anomalies over the NWP and East Asia shift northward and westward in 1988–2008 relative to those in 1966–86. Third, there are significant anomalous descending motions over South China and the East China Sea in 1988–2008, but anomalous vertical motion is weak in the above regions in 1966–86. Fourth, anomalous ascending motions over the tropical

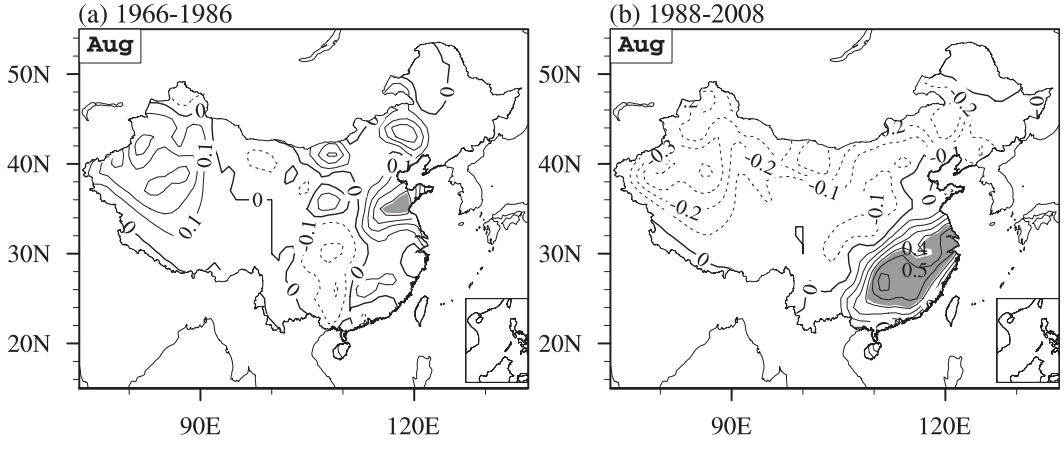

FIG. 4. Correlation of the DJF(0) Niño-3 index with the August hot-day numbers during (a) 1966–86 and (b) 1988–2008. The solid lines represent positive correlation, the dashed lines represent negative correlation, and the line interval is 0.1 in correlation. The shaded areas denote correlation reaching the 95% confidence level. The small inset map denotes the region of South China Sea.

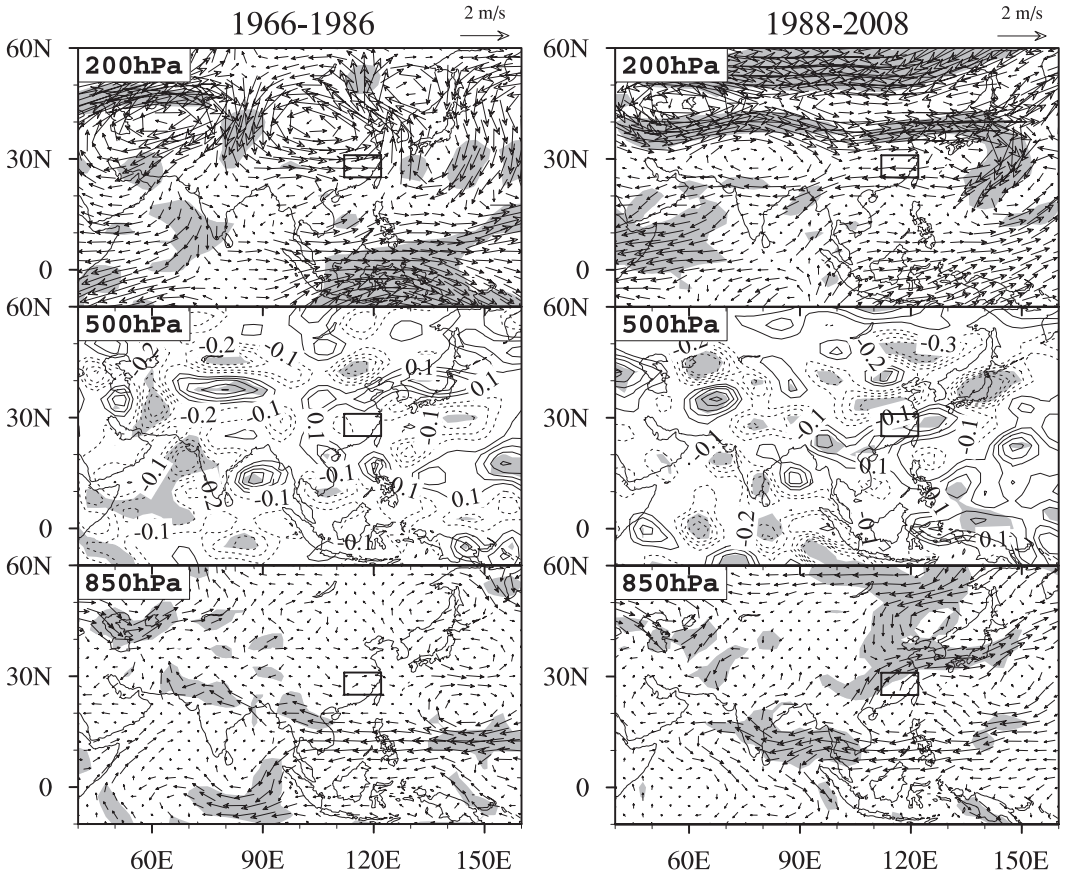

FIG. 5. Observed anomalies of 200-hPa winds, 500-hPa vertical velocity (×50), and 850-hPa winds obtained by regression on the normalized DJF(0) Niño-3 index for (left) 1966–86 and (right) 1988–2008. The wind scale is shown at the top of the panels. The rectangles represent the region of the SYRV. Shading denotes the 95% confidence level.

Indian Ocean shifted eastward from the former period to the latter period. Focusing on the SYRV, this region is located to the north side of low-level anomalous anticyclone and under the upper-level westerly anomalies in the former period but is located on the west side of the low-level anomalous anticyclone and under the influence of upper-level anomalous easterlies in the latter period. Moreover, anomalous descending motion over the SYRV is stronger in the latter period than in the former period.

b. The reasons for decadal change in ENSO-related circulation anomalies over SYRV in August

Figure 6 shows the correlation of August SST and tropospheric (850–200-hPa mean) temperature with the DJF(0) Niño-3 index. During 1966–86, a positive SST correlation is seen over the southwest tropical Indian Ocean, the equatorial central Indian Ocean, and the South China Sea (SCS). The tropospheric temperature correlation displays a Matsuno–Gill (Matsuno 1966; Gill 1980) pattern with the maximum correlation over the eastern tropical Indian Ocean. This suggests that equatorial central Indian Ocean SST anomalies are the important forcing for atmospheric circulation. During 1988–2008, positive SST correlation is mainly distributed in the north Indian Ocean and the South China Sea. The maximum positive correlation for tropospheric temperature is located over the north Indian Ocean, South Asia, and the equatorial western Pacific, which agree remarkably well with the theoretical solution corresponding to heating to the north of the equator in Gill (1980). This suggests that the north Indian Ocean SST anomalies play an important role in this period.

It is noted that a Kelvin wave wedge penetrates to the western Pacific along the equator in both periods (Fig. 6), which could induce a low-level anticyclone over the NWP (Fig. 5) according to Xie et al. (2009). Wu et al. (2010) demonstrated that the Indian Ocean–induced NWP anomalous anticyclone developed around the location of monsoon trough. However, the anticyclonic wind anomalies extend westward in 1988–2008 relative to 1966–86. This is possibly because of anomalous descending motion over the East China Sea and southeast

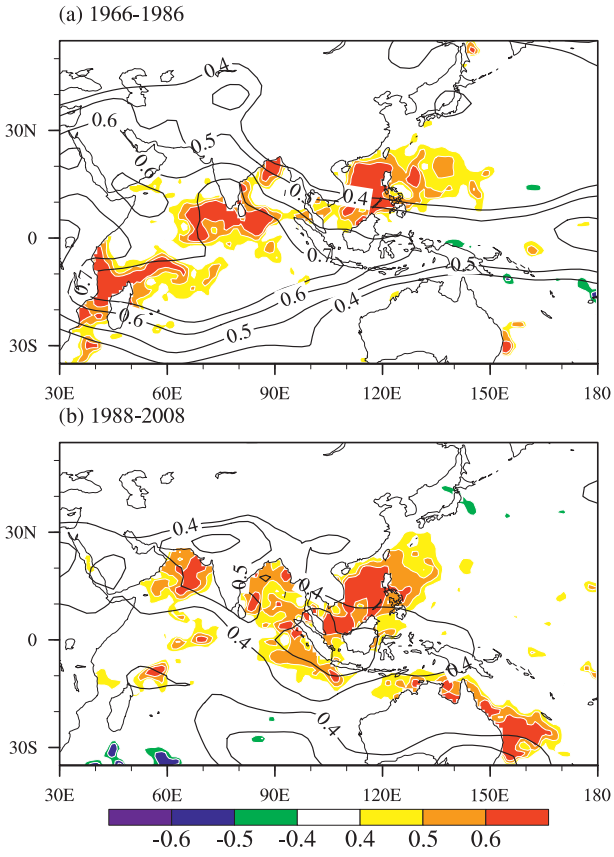

FIG. 6. Correlation of August SST (colors) and tropospheric temperature (vertical average from 850 to 200 hPa; contours for correlation ≥0.4) with the DJF(0) Niño-3 index during (a) 1966–86 and (b) 1988–2008.

China that could lead to low-level anticyclonic wind anomalies through divergence. The descending motion over the East China Sea and southeast China is possibly caused by upper easterly anomalies, which will be discussed later.

As the SST forcing has moved from the equatorial central Indian Ocean in the former period to the north Indian Ocean in the latter period, the response of atmospheric circulation has changed. Over the subtropical areas to the north of the Indian Ocean, the correlation for tropospheric temperature is more significant in 1988–2008 than in 1966–86. This indicates that the north Indian Ocean forcing poses a larger impact on the South Asia high than the equatorial central Indian Ocean forcing. The results are consistent with Qu and Huang (2012b), who identified that the north Indian Ocean SST plays an important role in strengthening the South Asia high. Thus, the ENSO-related South Asia high anomalies in 1988–2008 are more obvious than in 1966–86 (Fig. 5) and SYRV is controlled by westerly anomalies in August during the El Niño decaying phase in later period.

Figure 7 shows the correlations of 200-hPa streamfunction in August with the DJF(0) Niño-3 index and the wave-activity fluxes based on the regression of the 200-hPa winds on DJF(0) Niño-3 index for the two subperiods. The wave-activity flux, defined by Takaya and Nakamura (2001), is independent of wave phase and parallel to the local group velocity of stationary Rossby waves. During 1969–86, there exist notable wave-activity fluxes over the midlatitudes, which lead to zonal wave structure in the streamfunction correlation distribution from the Caspian Sea to the NWP, with negative correlations over the eastern part of the Asian continent. The wave pattern is similar to the circumglobal teleconnection identified by Ding and Wang (2005). During 1988–2008, the midlatitude wave-activity fluxes are weak; thus, the streamfunction correlation pattern is zonally elongated over the midlatitudes.

The different response of midlatitude wave activities to ENSO may be related to the change in ENSO-induced tropical Indian Ocean SST anomalies. According to Gill (1980), there exist Rossby wave tails in the west of tropical heating. Thus, the significant positive correlation of tropospheric temperature over the northwest Indian Ocean in both periods is related to the Rossby wave–type response. However, the tropospheric temperature anomalies over the northwest Indian Ocean extend farther northward and westward in the former period than in the latter period, possibly because the Rossby wave response to the equatorial central Indian Ocean SST anomalies during 1966–86 is stronger than that to the north Indian Ocean SST anomalies during 1988–2008. Consistent with tropospheric temperature anomalies, the ascending motions (Fig. 5) over the Arabian Sea are stronger in 1966–86 than in 1988–2008. Therefore, the ENSO-related midlatitude wave activities are stronger in the former period than in the latter period and SYRV is controlled by westerly anomalies located to the south part of anomalous cyclone over eastern China during the El Niño decaying phase.

Why is the distribution of August SST anomalies in the tropical Indian Ocean in the El Niño decaying year different in the two periods? Previous studies show that tropical Indian Ocean (TIO) warming is triggered by El Niño through an atmospheric bridge (Klein et al. 1999) and maintained by the local ocean–atmosphere interaction (Du et al. 2009). Figures 8a,b show the observed correlations with the DJF(0) Niño-3.4 SST index of SST and 850-hPa wind averaged zonally over the TIO (40°–100°E). In the north Indian Ocean, El Niño–induced SST warming persists longer during 1988–2008 than 1966–86, with the correlation staying above 0.6 in August in the latter period but falling below 0.5 in the former period. By contrast, El Niño–induced SST

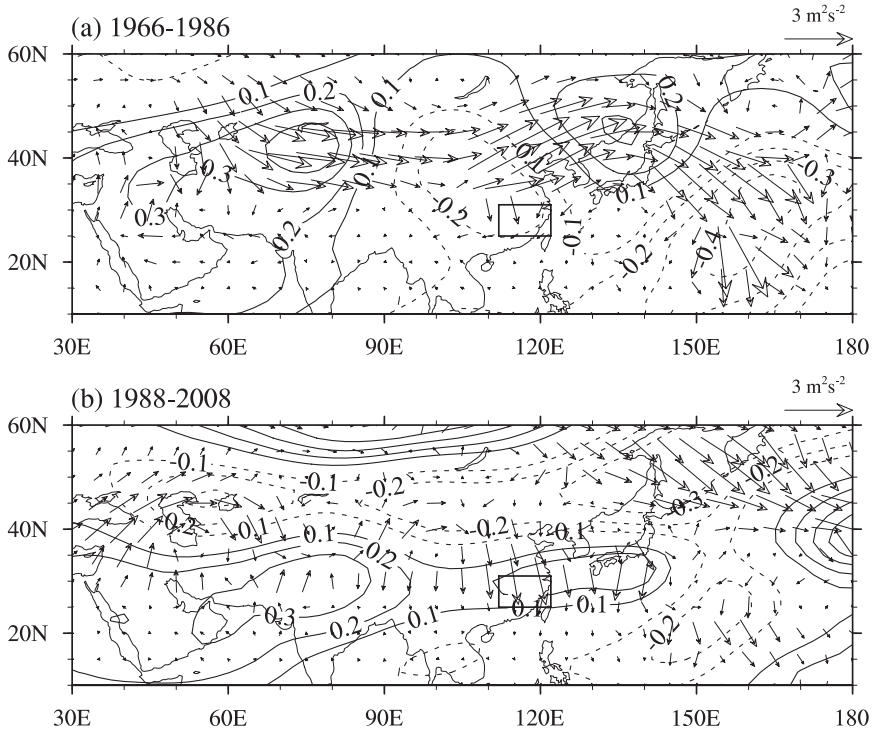

FIG. 7. Correlation of 200-hPa streamfunction (contours) in August with the DJF(0) Niño-3 index during (a) 1966–86 and (b) 1988–2008. The vectors show wave-activity fluxes for stationary Rossby wave based on the regression of 200-hPa winds on the normalized DJF(0) Niño-3 index. The rectangles represent the region of the SYRV.

warming in the south and equatorial Indian Ocean persists longer during 1966–86 than 1988–2008. During 1988–2008, an equatorially antisymmetric wind pattern develops in April and persists through August. Over the north Indian Ocean, the associated easterly wind anomalies act to warm SST after the onset of the southwest monsoon by reducing the prevailing winds and surface evaporation. During 1966–86, the antisymmetric wind pattern does not appear in spring, and the easterly wind anomalies are weak afterward over the north Indian Ocean, where SST anomalies decay rapidly, whereas strong westerly wind anomalies develop over the tropical south Indian Ocean, forming anticyclonic wind shear anomalies along their south flank, which may warm the tropical south Indian Ocean through triggering downwelling ocean Rossby waves. Thus, the change of El Niño–induced TIO SST anomalies from the former to the latter period possibly due to air–sea interaction in tropical Indian Ocean has experienced a decadal change in the late 1980s.

c. The ENSO-related adiabatic warming over SYRV in August

Since the air temperature over the Asian continent is higher than the neighboring oceanic regions, the ENSO-related upper-level easterly anomalies over the eastern part of China could lead to cold horizontal temperature advection. According to the omega equation, the cold horizontal temperature advection is conductive to descending motion. Indeed, the 200-hPa easterly belt is accompanied by anomalous descent at 500 hPa extending from the East China Sea to the northern part of the Indochinese peninsula during 1988–2008 (Fig. 5, right). Figure 9 shows the correlation of upper-level (400–200-hPa vertical average) vertical temperature advection and horizontal temperature advection in August with the DJF(0) Niño-3 index during the two subperiods. We average the advection for 400–200 hPa because the pattern of ENSO-related circulation anomalies is similar at these levels. During 1988–2008, there exists obvious cold temperature horizontal advection along 25°–30°N, extending from southwest China to the East China Sea. Correspondingly, adiabatic warming predominates along this belt. During 1966–86, by contrast, the horizontal temperature advection is weak, as is the vertical advection in the eastern part of China. Thus, the decadal change in descending motion over SYRV is possibly caused by the change in upper-level wind anomaly from westerly to easterly in the late 1980s.

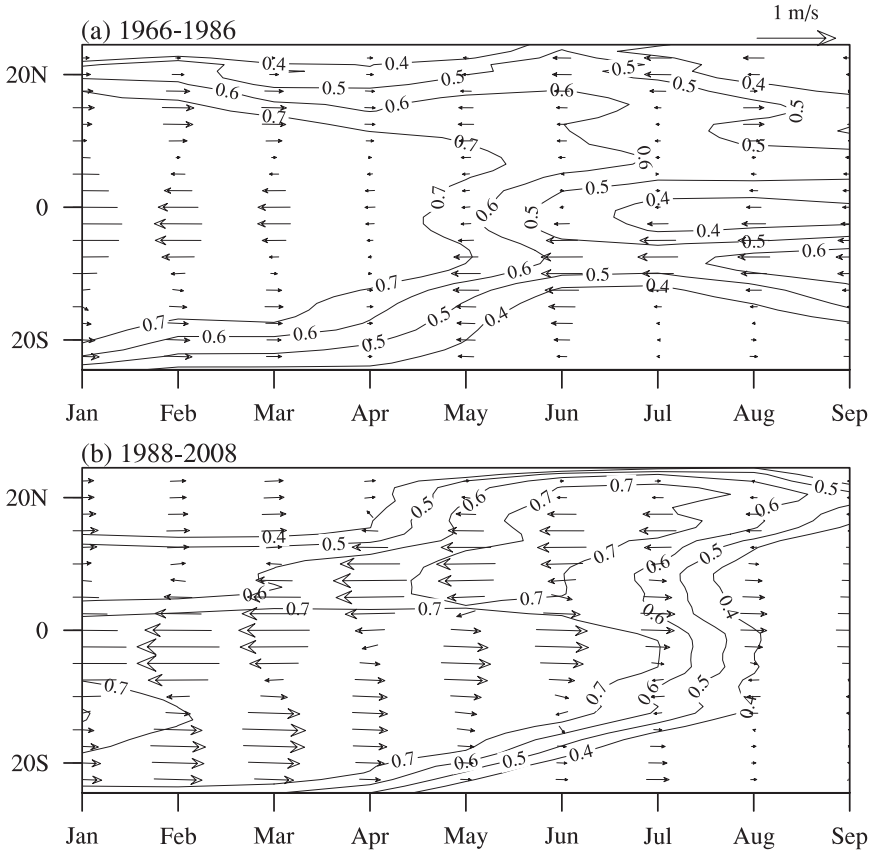

FIG. 8. Observed correlation (contours) between zonal-mean tropical Indian Ocean SST (40°–100°E) and the DJF(0) Niño-3 index and the regression (vector) of zonal-mean 850-hPa wind upon the Niño-3 index during (a) 1966–86 and (b) 1988–2008, as a function of calendar month and latitude.

Overall, El Niño–related north Indian Ocean warming during 1988–2008 leads to the strengthening and eastward extension of the South Asia high, and El Niño–related equatorial central Indian Ocean warming during 1966–86 induces an upper-level anomalous anticyclone over China through a midlatitude wave pattern. Thus, the SYRV is controlled by westerly anomalies in August during the El Niño decaying phase in the former period but by easterly anomalies in the latter period. The easterly anomalies could lead to descending motion over SYRV through cold horizontal temperature advection in the latter period. In addition, both the north Indian Ocean warming and equatorial central Indian Ocean warming can induce an anomalous anticyclone over the NWP through a Kelvin wave–type response and the NWP anticyclone extends westward possibly because of descending motion over the East China Sea and southeast China.

To further demonstrate the role of descent-related adiabatic warming, we perform a heat budget analysis. According to the atmospheric temperature tendency equation, the temperature anomalies are caused by atmospheric adiabatic and diabatic heating. Following the study of Yanai et al. (1973), we used the atmospheric apparent heat source Q_1 to represent the total diabatic heating (including radiation, latent heating, and surface heat flux),

$$Q_1 = C_p \frac{\partial T}{\partial t} - C_p(\omega\sigma - \mathbf{V}\cdot\nabla T), \qquad (1)$$

where C_p denotes the specific heat at constant pressure, T denotes the temperature, t denotes the time, ω denotes the vertical p velocity, $\sigma = (RT/C_pP) - (\partial T/\partial P)$ denotes the static stability, R denotes the gas constant, p denotes the pressure, $\mathbf{V}$ denotes the horizontal velocity vector, and ∇ denotes the horizontal gradient operator.

Figures 10 and 11 show the correlation of August low-level (vertical average from 1000 to 850 hPa) temperature anomalies T_a, temperature vertical advection V_adv, temperature horizontal advection H_adv, and Q_1 with the DJF(0) Niño-3 index during 1966–86 and 1988–2008, respectively. The contrast between the ENSO-related

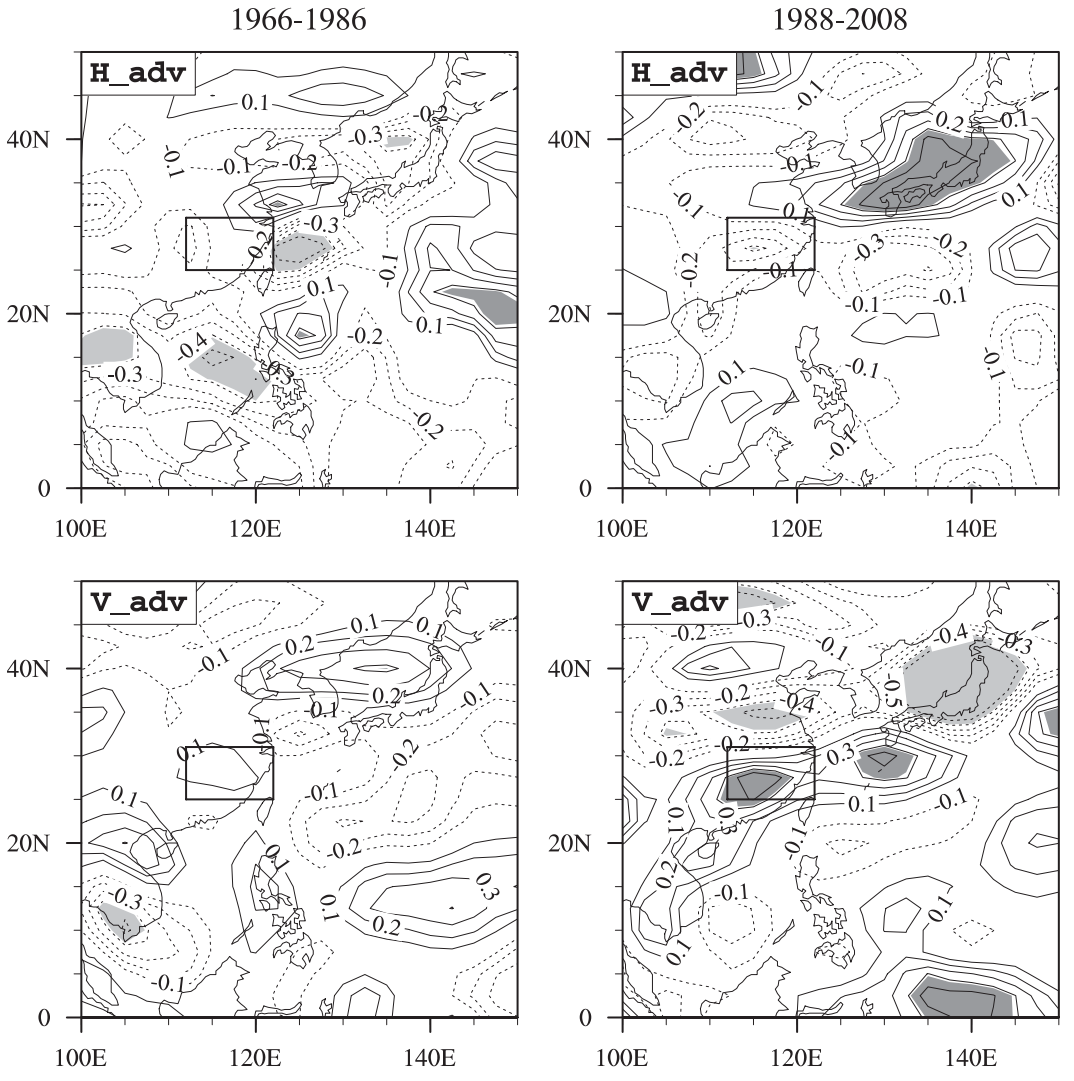

FIG. 9. Correlation of August upper-level (vertical average from 400 to 200 hPa) horizontal temperature advection H_adv and vertical temperature advection V_adv with the DJF(0) Niño-3 index during (left) 1966–86 and (right) 1988–2008. The shades denote 95% confidence level. The rectangles represent the region of the SYRV.

low-level temperature anomalies and atmospheric heating between the two subperiods is remarkable, especially over the SYRV.

During 1966–86, the most significant positive correlation for low-level air temperature is distributed in the Indochinese peninsula, the South China Sea, and the subtropical NWP. Thus, a low-level warm zone extends from the Indochinese peninsula to the subtropical NWP in August during El Niño decaying years. The contribution of different heating processes to low-level air temperature anomalies are investigated through discussing whether the correlation for T_a is of the same sign as or opposite to the correlation for each heating process. The heating processes positively contribute to the low-level temperature anomalies where the correlation has the same sign. In this way, we identified that temperature anomalies over the eastern SCS and NWP are mainly contributed by the temperature vertical advection, the temperature anomalies over the Indochinese peninsula are mainly contributed by the temperature horizontal advection, and the temperature anomalies in the tropical western Pacific and the SCS are mainly contributed by the diabatic heating.

During 1988–2008, the area with significant correlation for T_a extends farther northward when compared with the period 1966–86. Beside the warm belt from the Indochinese peninsula to the subtropical NWP, there also exists a warm belt from eastern China to the East China Sea during El Niño decaying years. The correlation for V_adv is significant and positive over eastern

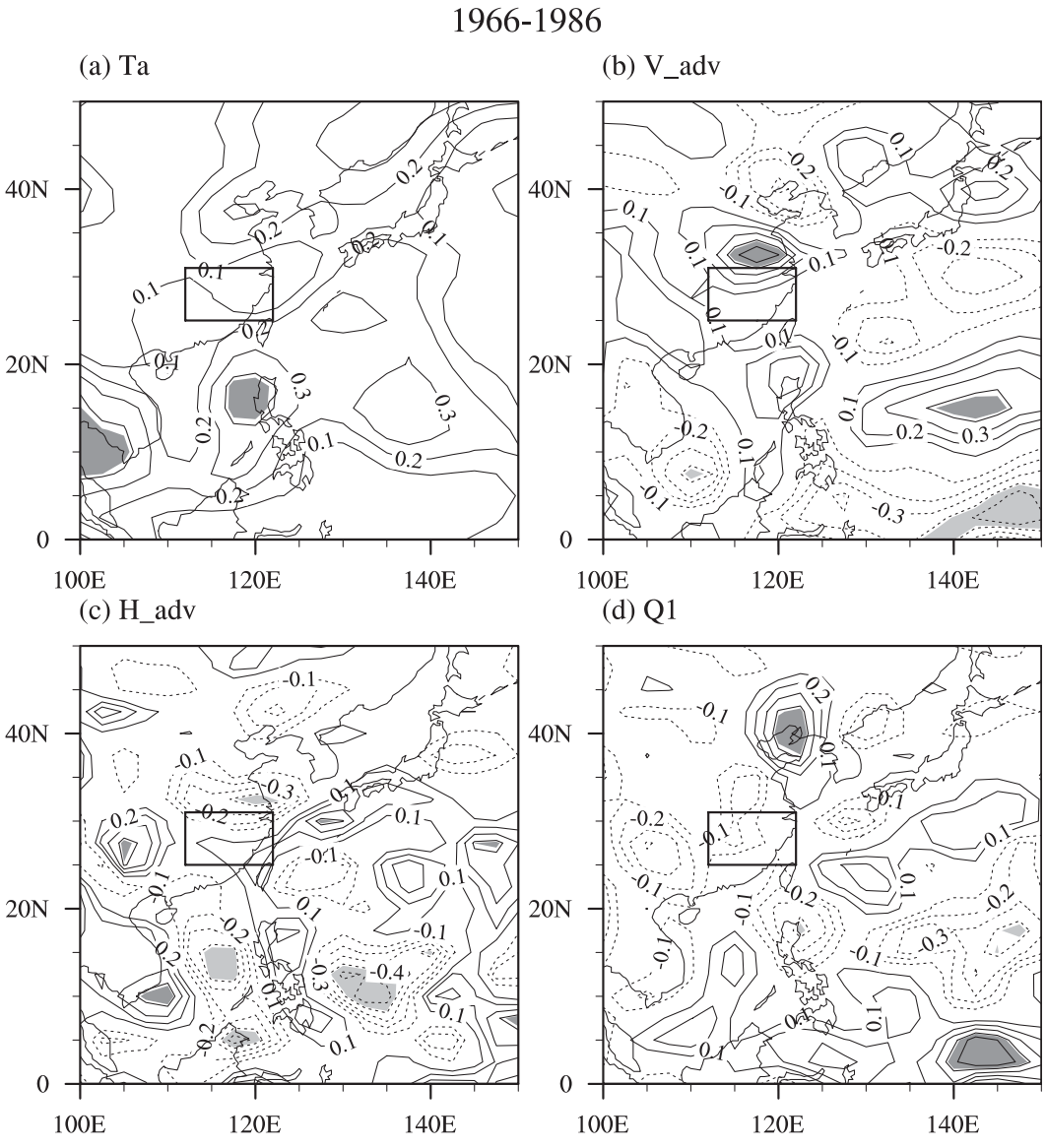

FIG. 10. Correlation of low-level (vertical average from 1000 to 850 hPa) (a) air temperature, (b) vertical temperature advection, (c) horizontal temperature advection, and (d) atmospheric apparent heat source with the DJF(0) Niño-3 index during 1966–86. The solid lines represent positive correlation, the dashed lines represent negative correlation, and the line interval is 0.1 in correlation. The rectangles represent the region of the SYRV. Shading denotes the 95% confidence level.

China and the East China Sea, but that for H_adv and Q_1 is negative in the above regions. This indicates that the warm belt from eastern China to the East China Sea mainly results from descent-induced warming. Focusing on the SYRV, the correlation for V_adv is significant and positive in most part of this region, the correlation for H_adv is negative in this region, and the correlation for Q_1 is weak in most part of this region. Therefore, the ENSO-related August low-level air temperature anomalies over SYRV are mainly contributed by vertical temperature advection during 1988–2008. Previous study suggests that the change of hot-day numbers and mean temperature are consistent. Therefore, the August SYRV hot-day numbers are expected to be above normal (below normal) during the El Niño (La Niña) decaying year in the latter period but are not linearly related to ENSO in the former period.

5. Model studies

This section uses atmospheric general circulation model (GCM) experiments to test the hypothesis that

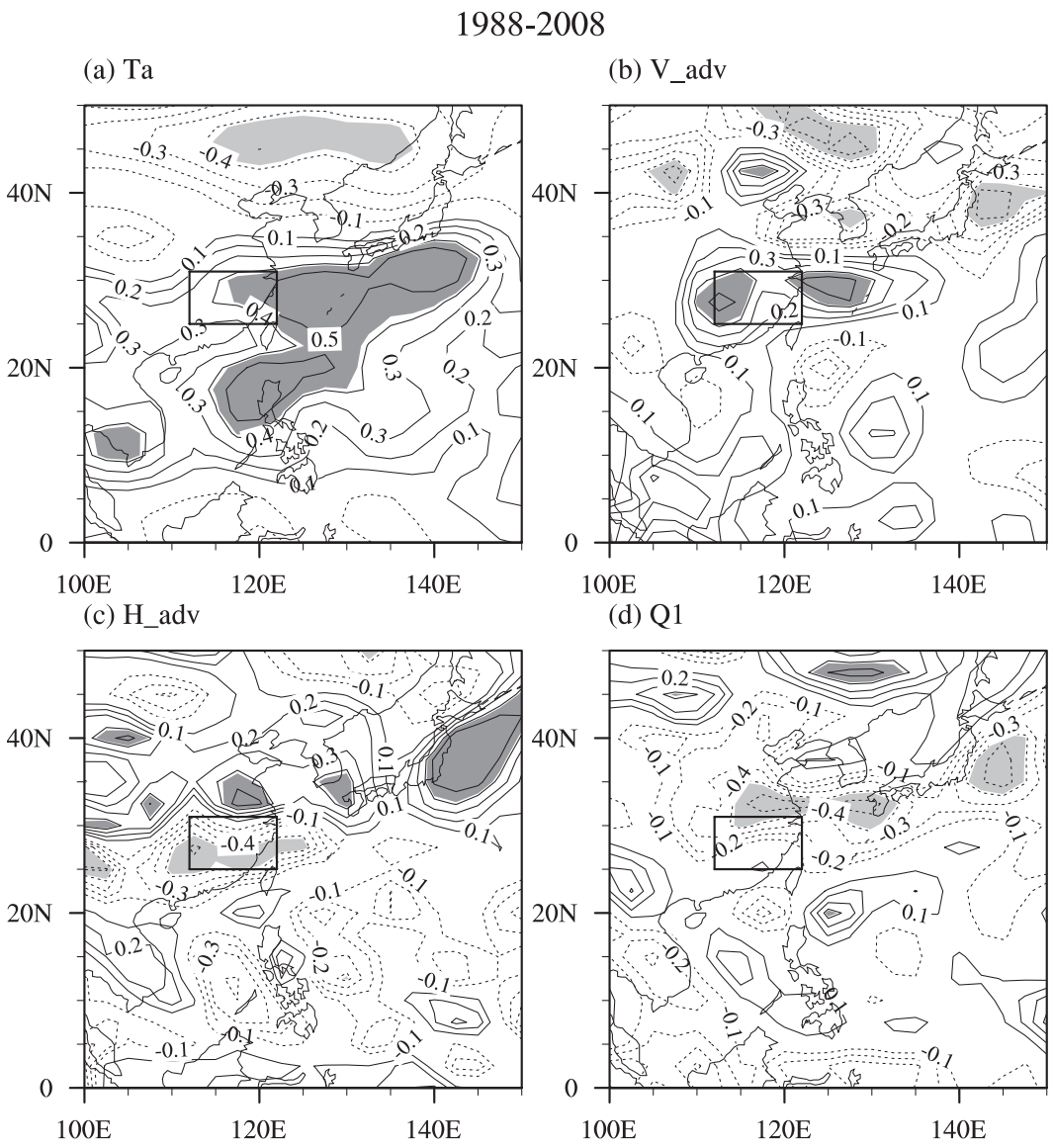

FIG. 11. Correlation of low-level (vertical average from 1000 to 850 hPa) (a) air temperature, (b) vertical temperature advection, (c) horizontal temperature advection, and (d) atmospheric apparent heat source with the DJF(0) Niño-3 index during 1988–2008. The solid lines represent positive correlation, the dashed lines represent negative correlation, and the line interval is 0.1 in correlation. The rectangles represent the region of the SYRV. Shading denotes the 95% confidence level.

the change of ENSO-related circulation anomalies over East Asia from the former period to the latter period is caused by different SST anomalies over the Indian Ocean. The atmospheric GCM used in this study is the ECHAM5.4, the latest Hamburg version of the European Centre for Medium-Range Weather Forecasts (ECMWF) model. Documentation of various aspects of this model may be found in Roeckner et al. (2003). We use a version with triangular truncation at zonal wavenumber 63 (T63; equivalent to 1.9° horizontal resolution) and 19 sigma levels in the vertical.

The following three experiments have been performed using the above atmospheric GCM in this study: control experiment EXP_CTL and sensitivity experiments EXP_PRE and EXP_POST. In the EXP_CTL run, the model is forced with observed monthly climatology of SST and sea ice. In the EXP_PRE run, SST anomalies (shown in Fig. 12a) have been added to the tropical Indian Ocean, which are twice the regression of

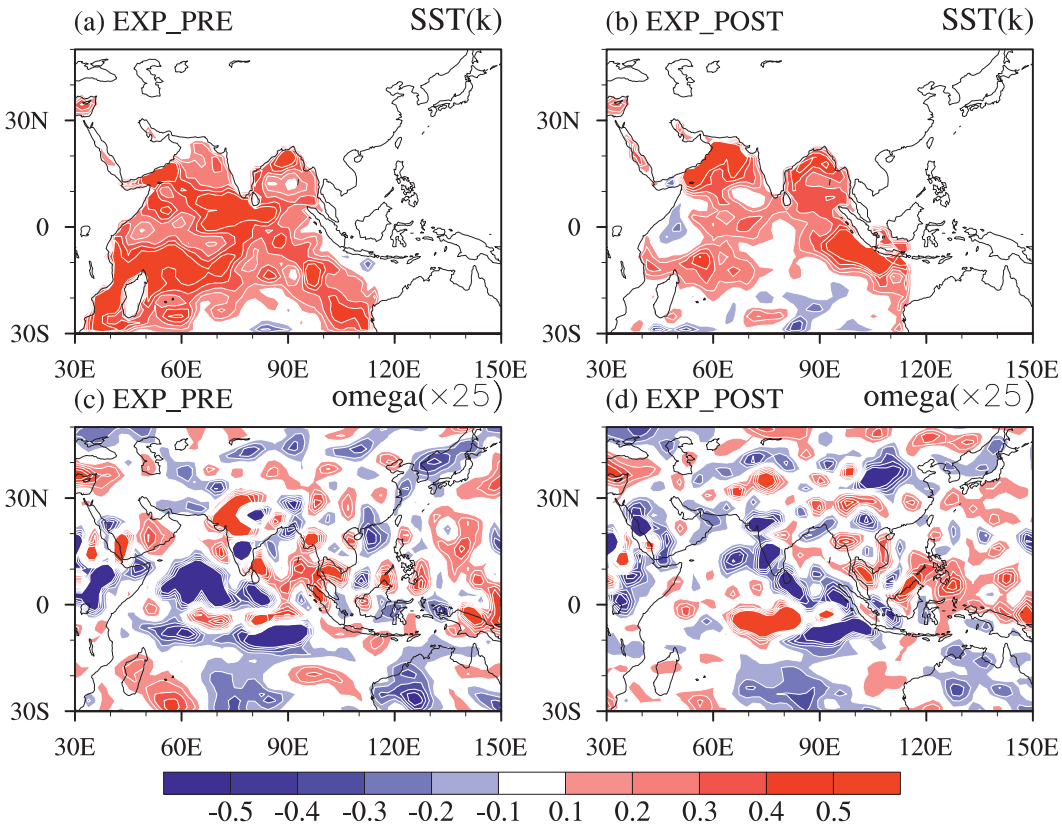

FIG. 12. Anomalies of (top) SST and (bottom) 500-hPa vertical velocity (×25) in the (a),(c) EXP_PRE and (b),(d) EXP_POST atmospheric GCM runs obtained by subtracting the corresponding climatology in the EXP_CTL run.

August SST on normalized DJF(0) Niño-3.4 index in 1966–86. In the EXP_POST run, the imposed SST anomalies (shown in Fig. 12b) are calculated the same way as the EXP_PRE run, except for basing on the data in 1988–2008. All the three experiments are run for 15 yr.

Figures 12c,d show anomalies of August 500-hPa vertical motions in EXP_PRE and EXP_POST, which are obtained by subtracting the corresponding climatology in the EXP_CTL run. All the analyses are based on 15-yr ensemble means. In the EXP_PRE run, there are ascent motion anomalies over much of the western and central Indian Ocean, and descent motion anomalies over the equatorial Indian Ocean, north Indian Ocean, and eastern Indian Ocean. Over the northwest Pacific, there are weak descent motion anomalies over the subtropical region and a weak ascent motion belt from South China to North Korea. In the EXP_POST run, there are ascent motion anomalies over much of the eastern Indian Ocean and the regions around the Indian subcontinent and descent motion anomalies over the equatorial central Indian Ocean. Over the northwest Pacific, there are descent motion anomalies around the Philippine Islands and a weak descent motion belt in the latitude around 30°N. Focusing on the SYRV regions, there are descent motion anomalies in the EXP_POST run but weak vertical motion anomalies in the EXP_PRE run, consistent with observations (Fig. 5).

Furthermore, we examine the 200- and 850-hPa wind anomalies and tropospheric vertical average temperature anomalies in the EXP_PRE and EXP_POST runs (Fig. 13). In the EXP_PRE run, at 200 hPa, there are westerly wind anomalies over the eastern Indian Ocean and equatorial western Pacific, easterly wind anomalies over the western Indian Ocean and Africa, and zonal wave structure wind anomalies over the midlatitudes, with an anomalous cyclone over China. At 850 hPa, there are easterly wind anomalies over the western Pacific and eastern Indian Ocean, westerly anomalies over the western Indian Ocean and Africa, and anticyclone anomalies over the northwest Pacific with the center over the east of Japan. Consistent with wind anomalies, the tropospheric temperature anomalies display a Matsuno–Gill pattern over the tropical Indian Ocean, with a head penetrating into the western Pacific. Compared with the observations in 1966–86 (Figs. 5, 6), the

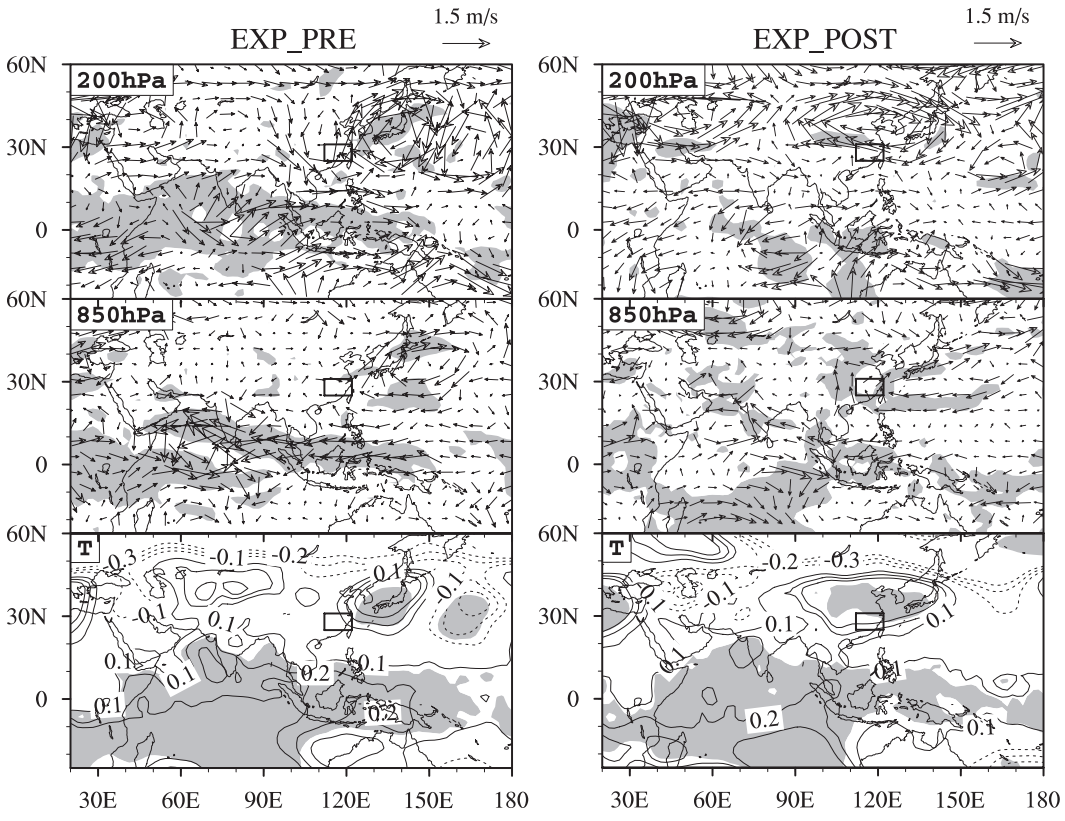

FIG. 13. Anomalies of August wind velocity (m s^{-1}; vectors) at 200- and 850-hPa winds and tropospheric temperature (vertical average from 850 to 200 hPa) in the EXP_PRE and EXP_POST atmospheric GCM runs by subtracting the EXP_CTL atmospheric GCM run. Shading denotes the 95% confidence level. The rectangles represent the region of the SYRV.

ensemble mean of EXP_PRE simulations can capture the Matsuno–Gill pattern circulation anomalies over TIO, the 200-hPa zonal wave structure wind anomalies over midlatitudes, and the 850-hPa anticyclone anomalies over NWP.

In the EXP_POST run, the model captures the main character of the observed El Niño–related circulation anomalies during 1988–2008. At 200 hPa, there are westerly wind anomalies over the Maritime Continent and easterly wind anomalies over the western Indian Ocean and Africa. Over East Asia, the 200-hPa wind anomalies display anticyclone anomalies that extend from China to Japan, suggesting that the South Asia high is enhanced. At 850 hPa, there are easterly wind anomalies extending from the equatorial western Pacific to the Arabian Sea, westerly wind anomalies over the western Indian Ocean, and anticyclone anomalies over NWP extending from the eastern part of China to the central Pacific. There are warm tropospheric temperature anomalies over the tropical Indian Ocean, featuring a Matsuno–Gill pattern, and a warm tongue extending from the Indian Ocean to east China, possibly caused by north Indian Ocean heating. Over the region of SYRV, there are 200-hPa easterly wind anomalies, which is in favor of descent motions.

Overall, although there are some differences between simulations and observations in detail, the ensemble means of the EXP_PRE and EXP_POST experiments can capture the main character of observed August circulation anomalies over the tropical Indian Ocean, NWP, and East Asia during El Niño decaying years in 1966–86 and 1988–2008, respectively. The results confirm that the decadal change of ENSO-related circulation anomalies over East Asia in the late 1980s is partly caused by the different response of Indian Ocean SST anomalies to ENSO in two subperiods.

6. The possible factors for August SYRV HTE anomalies before the late 1980s

The previous section suggests that the impact of ENSO on the August SYRV HTEs is weak before the late 1980s. To address the plausible causes of August SYRV HTEs anomalies before the late 1980s, we

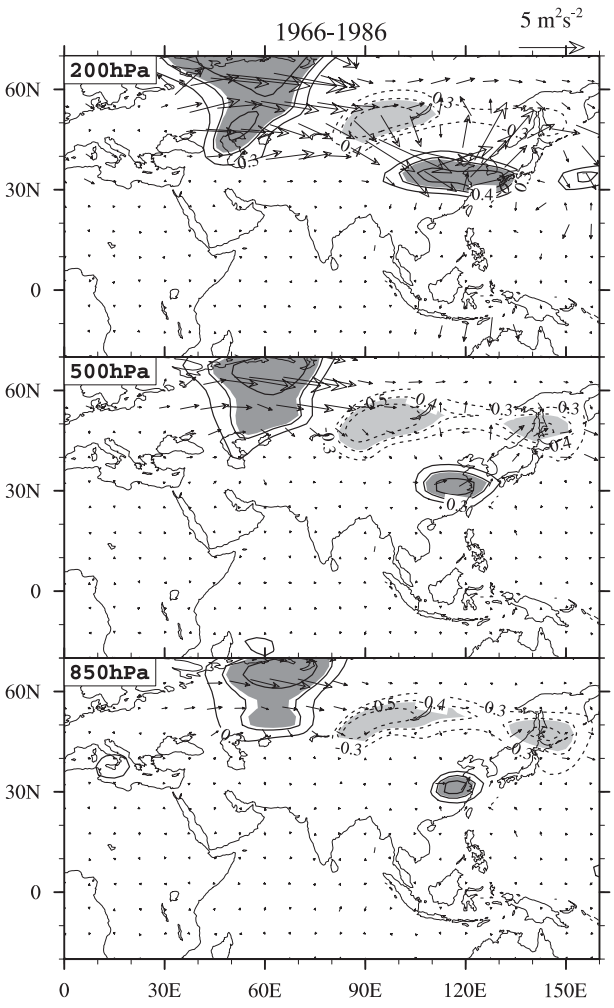

FIG. 14. Correlation of geopotential height (contours) at 200, 500, and 850 hPa with HTE_PC1 (time series of first leading SVD mode for HTEs) during 1966–86. The vectors show wave-activity flux for stationary Rossby wave based on the regression of August winds on the normalized DJF(0) Niño-3 index. Shading denotes correlation reaching the 95% confidence level.

investigate the distribution of circulation, wave activities, and SST anomalies associated with late summer SYRV HTE variation in 1966–86.

Figures 14a–c show the August geopotential height correlations with PC1 of the HTE SVD mode at 200, 500, and 850 hPa and their associated wave-activity fluxes during 1966–86. Significant correlations are confined to the midlatitudes, featuring wave structure with alternating positive and negative anomalies at all levels. Over the Asian continent, the above normal HTEs in the SYRV region correspond to high pressure anomalies over the eastern part of China, low pressure anomalies around the Lake of Baikal, and high pressure anomalies over the Urals. The significant positive correlations over SYRV suggest that this region is vulnerable to HTEs when they are controlled by high anomalies. Consistent with the geopotential height anomalies, there exist wave-activity fluxes from the Eurasian continent to the region around SYRV. This indicates that the high anomalies over SYRV are partly affected by midlatitude and high-latitude wave-activity anomalies in this period. Moreover, there are no obvious lead–lag correlations between tropical SST and HTE_PC1 (figure not shown), suggesting that the August SYRV HTEs are not linearly related to tropical SST forcing in this period. Thus, the August SYRV HTEs anomalies are possibly caused by the atmospheric internal wave activities.

7. Summary and discussion

The relationship of interannual variations of the August SYRV hot-day number with ENSO experienced an obvious change in the late 1980s. After the late 1980s, the August SYRV hot-day number tends to be more (less) than normal during the El Niño (La Niña) decaying year, whereas before the late 1980s the relationship is weak. Present analysis shows that the decadal change in the relationship possibly results from the change in ENSO-related East Asia circulation anomalies. After the late 1980s, the descending motion over SYRV is significant in August during El Niño decaying years, whereas before the late 1980s the vertical motion over SYRV is weak. Therefore, the SYRV is controlled by El Niño–related adiabatic warming during the 1989–2008, which in turn leads to above normal hot days in this region. This may be the reason that the relation between ENSO and August SYRV HTEs is strengthened after the late 1980s.

The change in ENSO-related circulation anomalies may be attributed to the differences of El Niño–induced tropical Indian Ocean SST anomalies between the two periods. A previous study shows that El Niño–induced tropical Indian Ocean warming can persist to boreal summer (Du et al. 2009). However, the detailed distribution of August SST anomalies in the tropical Indian Ocean in the El Niño decaying year are different in the two periods. During 1966–86, El Niño–related SST anomalies are mainly distributed in the equatorial central and southwest Indian Ocean, which lead to ascending motion over the Arabian Sea. The ascending motion over the above region excites midlatitude wave activities, leading to an anomalous cyclone over China. Thus, the SYRV is controlled by upper-level westerly anomalies in the period of 1966–86. During 1988–2008, the SST anomalies are mainly distributed in the eastern and north Indian Ocean, and the ascending motion over the Arabian Sea is weak. Thus, the midlatitude wave activities are weak. Moreover, the South Asia

high is strengthened possibly because of the north Indian Ocean warming. Therefore, the SYRV is controlled by upper-level easterlies during 1988–2008. According to the omega equation, the cold horizontal temperature advection resulted from easterlies over east China is conductive to descending motion. Therefore, the ENSO-related descending motion over SYRV is stronger in the latter period than in the former period.

Moreover, we find that the August SYRV HTE anomalies in the former period are closely related to midlatitude and high-latitude wave-activity anomalies but are not significantly related to tropical SST forcing. Thus, the August SYRV HTEs in the former period are possibly caused by atmospheric internal variation.

This study mainly focused on the change in ENSO-related tropical Indian Ocean SST anomalies and impacts on the relationship between ENSO and the August SYRV HTE anomalies. Previous studies indicated that the mean state of summer climate in China and NWP has experienced a decadal change in the late 1980s. For example, the western Pacific subtropical high extended westward after the late 1980s (Zhang et al. 2008). Whether the decadal change in the relationship between ENSO and the August SYRV HTE anomalies is related to the decadal change in the mean circulation deserves further study in the future.

Acknowledgments. The authors wish to thank Prof. Ronghui Huang and Prof. Shang-Ping Xie for their helpful discussion and three anonymous reviewers for their useful comments. This work is supported by National Basic Research Program of China (973 Program) under Grant 2012CB955604 and 2011CB309704, Strategic Priority Research Program—Climate Change: Carbon Budget and Relevant Issues of the Chinese Academy of Sciences (Grant XDA05090101), and the National Natural Science Foundation of China (Grants 41205049 and 41275083).

REFERENCES

Ding, Q., and B. Wang, 2005: Circumglobal teleconnection in the Northern Hemisphere summer. *J. Climate,* **18,** 3483–3505.

Du, Y., S.-P. Xie, G. Huang, and K. Hu, 2009: Role of air–sea interaction in the long persistence of El Niño–induced north Indian Ocean warming. *J. Climate,* **22,** 2023–2038.

Easterling, D. R., G. A. Meehl, C. Parmesan, S. A. Changnon, T. R. Karl, and L. O. Mearns, 2000: Climate extremes: Observations, modeling, and impacts. *Science,* **289,** 2068–2074.

Fu, C., and D. Ye, 1988: The tropical very low-frequency oscillation on interannual scale. *Adv. Atmos. Sci.,* **5,** 369–388.

Gill, A. E., 1980: Some simple solutions for heat-induced tropical circulation. *Quart. J. Roy. Meteor. Soc.,* **106,** 447–462.

Hu, K., G. Huang, and R. Huang, 2011: The impact of tropical Indian Ocean variability on summer surface air temperature in China. *J. Climate,* **24,** 5365–5377.

——, ——, X. Qu, and R. Huang, 2012: The impact of Indian Ocean variability on high temperature extremes across the southern Yangtze River valley in late summer. *Adv. Atmos. Sci.,* **29,** 91–100.

Huang, G., K. Hu, and S. P. Xie, 2010: Strengthening of tropical Indian Ocean teleconnection to the northwest Pacific since the mid-1970s: An atmospheric GCM study. *J. Climate,* **23,** 5294–5304.

——, X. Qu, and K. M. Hu, 2011: The impact of the tropical Indian Ocean on South Asian high in boreal summer. *Adv. Atmos. Sci.,* **28,** 421–432.

Huang, R., and Y. Wu, 1989: The influence of ENSO on the summer climate change in China and its mechanism. *Adv. Atmos. Sci.,* **6,** 21–32.

Kalnay, E., and Coauthors, 1996: The NCEP/NCAR 40-Year Reanalysis Project. *Bull. Amer. Meteor. Soc.,* **77,** 437–471.

Klein, S. A., B. J. Soden, and N. C. Lau, 1999: Remote sea surface temperature variations during ENSO: Evidence for a tropical atmospheric bridge. *J. Climate,* **12,** 917–932.

Li, S., J. Lu, G. Huang, and K. Hu, 2008: Tropical Indian Ocean basin warming and East Asian summer monsoon: A multiple AGCM study. *J. Climate,* **21,** 6080–6088.

Li, Z., and Z. W. Yan, 2009: Homogenized daily mean/maximum/minimum temperature series for China from 1960-2008. *Atmos. Oceanic Sci. Lett.,* **2,** 237–243.

Mann, H. B., 1945: Nonparametric tests against trend. *Econometrica,* **13,** 245–259.

Matsuno, T., 1966: Quasi-geostrophic motions in the equatorial area. *J. Meteor. Soc. Japan,* **44,** 25–43.

Qu, X., and G. Huang, 2012a: Impacts of tropical Indian Ocean SST on the meridional displacement of East Asian jet in boreal summer. *Int. J. Climatol.,* **32,** 2073–2080.

——, and ——, 2012b: An enhanced influence of tropical Indian Ocean on the South Asia high after the late 1970s. *J. Climate,* **25,** 6930–6941.

Rayner, N. A., D. E. Parker, E. B. Horton, C. K. Folland, L. V. Alexander, D. P. Rowell, E. C. Kent, and A. Kaplan, 2003: Global analyses of sea surface temperature, sea ice, and night marine air temperature since the late nineteenth century. *J. Geophys. Res.,* **108,** 4407, doi:10.1029/2002JD002670.

Roeckner, E., and Coauthors, 2003: Atmospheric general circulation model ECHAM5: Part I. Max-Planck-Institut für Meteorlogie Rep. 349, 140 pp.

Schär, C., and G. Jendritzky, 2004: Hot news from summer 2003. *Nature,* **432,** 559–560.

Takaya, K., and H. Nakamura, 2001: A formulation of a phase-independent wave-activity flux for stationary and migratory quasigeostrophic eddies on a zonally varying basic flow. *J. Atmos. Sci.,* **58,** 608–627.

Tan, J., Y. Zheng, G. Song, L. Kalkstein, A. Kalkstein, and X. Tang, 2007: Heat wave impacts on mortality in Shanghai, 1998 and 2003. *Int. J. Biometeor.,* **51,** 193–200.

Wang, B., R. G. Wu, and X. H. Fu, 2000: Pacific–East Asian teleconnection: How does ENSO affect East Asian climate? *J. Climate,* **13,** 1517–1536.

Wei, K., and W. Chen, 2009: Climatology and trends of high temperature extremes across China in summer. *Atmos. Oceanic Sci. Lett.,* **2,** 153–158.

——, and ——, 2011: An abrupt increase in the summer high temperature extreme days across China in the mid-1990s. *Adv. Atmos. Sci.,* **28,** 1023–1029.

Wu, B., T. Li, and T. Zhou, 2010: Relative contributions of the Indian Ocean and local SST anomalies to the maintenance of the western North Pacific anomalous anticyclone during the El Niño decaying summer. *J. Climate,* **23,** 2974–2986.

Wu, R., and B. Wang, 2002: A contrast of the East Asian summer monsoon–ENSO relationship between 1962–77 and 1978–93. *J. Climate,* **15,** 3266–3279.

——, Z. Z. Hu, and B. P. Kirtman, 2003: Evolution of ENSO-related rainfall anomalies in East Asia. *J. Climate,* **16,** 3742–3758.

——, S. Yang, S. Liu, L. Sun, Y. Lian, and Z. Gao, 2010: Changes in the relationship between northeast China summer temperature and ENSO. *J. Geophys. Res.,* **115,** D21107, doi:10.1029/2010JD014422.

Xie, S. P., K. M. Hu, J. Hafner, H. Tokinaga, Y. Du, G. Huang, and T. Sampe, 2009: Indian Ocean capacitor effect on Indo–western Pacific climate during the summer following El Niño. *J. Climate,* **22,** 730–747.

——, Y. Du, G. Huang, X. T. Zheng, H. Tokinaga, K. Hu, and Q. Liu, 2010: Decadal shift in El Niño influences on Indo–western Pacific and East Asian climate in the 1970s. *J. Climate,* **23,** 3352–3368.

Yanai, M., S. Esbensen, and J. H. Chu, 1973: Determination of bulk properties of tropical cloud clusters from large-scale heat and moisture budgets. *J. Atmos. Sci.,* **30,** 611–627.

Yang, J., Q. Liu, S.-P. Xie, Z. Liu, and L. Wu, 2007: Impact of the Indian Ocean SST basin mode on the Asian summer monsoon. *Geophys. Res. Lett.,* **34,** L02708, doi:10.1029/2006GL028571.

Zhai, P., A. Sun, F. Ren, X. Liu, B. Gao, and Q. Zhang, 1999: Changes of climate extremes in China. *Climatic Change,* **42,** 203–218.

Zhang, R., A. Sumi, and M. Kimoto, 1996: Impact of El Niño on the East Asian monsoon: A diagnostic study of the '86/87 and '91/92 events. *J. Meteor. Soc. Japan,* **74,** 49–62.

——, B. Wu, P. Zhao, and J. Han, 2008: The decadal shift of the summer climate in the late 1980s over eastern China and its possible causes. *Acta Meteor. Sin.,* **4,** 435–445.